

# New TiC/Co<sub>1.5</sub>CrFeNi<sub>1.5</sub>Ti<sub>0.5</sub> Cermet with Slow TiC Coarsening During Sintering

CHUN-MING LIN,<sup>1</sup> CHE-WEI TSAI,<sup>1</sup> SHENG-MIN HUANG,<sup>1</sup>  
CHIH-CHAO YANG,<sup>2</sup> and JIEN-WEI YEHL<sup>1,3</sup>

1.—Department of Materials Science and Engineering, National Tsing Hua University, Hsinchu 30013, Taiwan. 2.—Green Energy & Eco-Technology System Center, ITRI South Campus, Industrial Technology Research Institute, Tainan 70955, Taiwan. 3.—e-mail: jwyeh@mx.nthu.edu.tw

New TiC/Co<sub>1.5</sub>CrFeNi<sub>1.5</sub>Ti<sub>0.5</sub> cermet was developed by exploiting the advantages of the high-entropy alloy (HEA) binder. A much finer grain structure and thus improved hardness–toughness combination were obtained as compared with two traditional binders, Ni and Ni<sub>13</sub>Mo<sub>7</sub>. From the coarsening behavior of TiC grains, the coarsening process of TiC in these three binders is diffusion-controlled. The activation energy of TiC + 20%Co<sub>1.5</sub>CrFeNi<sub>1.5</sub>Ti<sub>0.5</sub> is the highest and that of TiC + 20%Ni is the lowest. The high activation energy of the Co<sub>1.5</sub>CrFeNi<sub>1.5</sub>Ti<sub>0.5</sub> binder was attributable to its high content of carbon-strong-binding elements, Cr and Ti, and cooperative diffusion and higher packing density of multiple different-sized atoms. Low diffusion coefficient, low surface energy of TiC grains, and low solubility of Ti in the HEA liquid explain the slow coarsening of TiC grains. This study demonstrates that Co<sub>1.5</sub>CrFeNi<sub>1.5</sub>Ti<sub>0.5</sub> is an excellent HEA binder for TiC cermets.

## INTRODUCTION

Liquid phase sintering (LPS) is an advantageous sintering method for cemented carbides and cermets. The advantages of LPS over solid-state sintering include faster sintering rates and effective densification for final products. It is well known that binder material, grain size and morphology of ceramic reinforcements, and overall densification have a pronounced influence on mechanical properties and performance of such composite tool materials.<sup>1,2</sup> Improvement of component materials and microstructure evolution during LPS are thus of great interest from both application and scientific standpoints. Microstructural evolution during LPS has been conducted for systems such as mixed oxides,<sup>3,4</sup> heavy-metal alloys,<sup>5,6</sup> and cemented carbides/cermets.<sup>7–10</sup> Grain coarsening, known also as Ostwald ripening, has been described by the Lifshitz, Slyozov, and Wagner (LSW) theory<sup>11,12</sup> and can be classified into diffusion-controlled and reaction-controlled processes. From the Gibbs–Thomson effect,<sup>13</sup> the solubility of the liquid matrix near the solid grains increases with the curvature of the solid grains. Accordingly, a concentration gradient is established between larger and smaller grains,

which makes small grains incline to dissolve into the liquid matrix and then precipitate onto the larger ones. The average grain size is therefore increased with sintering time. The mode of coarsening, i.e., diffusion- or reaction-controlled, can be ascertained from the volume fraction of liquid matrix<sup>14,15</sup> and the shape of grains that have undergone coarsening.<sup>10,15–17</sup> In the diffusion-controlled process, the coarsening rate is expected to decrease as the volume fraction of the liquid matrix increases because the diffusion path length is increased. On the other hand, in the reaction-controlled case, the coarsening rate remains constant for different volume fractions of the liquid as the jumping rate of atoms through the solid/liquid interface determines the growth rate. Regarding shape, grains are found to coarsen with a spherical shape if the solid/liquid interface is atomically rough and has numerous dangling bonds. Thus, spherically coarsened grains are indicative of a diffusion-controlled process. Faceted particles, however, indicate a reaction-controlled process, in which the attachment of an atom to a smooth solid surface will result in the formation of excess dangling bonds and, thus, raises the total chemical potential. For this case, grain growth precedes by

the generation of ledge sources, such as two-dimensional surface nucleation and spiral growth of screw dislocations. Such growth processes are known as lateral growth. As for the mixed-shape morphology, Moon et al.<sup>15</sup> investigated the 70NbC-30Co-xB(wt.%) system having mixed interfaces in a liquid matrix and reveal its kinetics type. The NbC grains in the sample without B addition are mostly well faceted with a slight corner and edge-rounded cube in three-dimensional shape. With the addition of 2.3 wt.% B, the tendency to edge rounding of the grains intensified, and the grain shape in the sample containing 3 wt.% B is spherical. They noted that small grains are almost spherical even for the case without B addition. They concluded that the growth kinetics of NbC grains, whether cubes with rounded edges or spheres, fitted well the LSW kinetic equation of diffusion control.<sup>11,12,15</sup> This study completes the rules for judging kinetics type from different kinds of grain shape. To inhibit coarsening and preserve a fine microstructure, specific additions, referred to as grain growth inhibitors or grain refiners, have been introduced during LPS. In the well-known case of WC/Co cemented carbides, VC, Cr<sub>3</sub>C<sub>2</sub>, and (Nb, Ta)C have been added as grain refiners.<sup>1,18</sup> For TiC/Ni cermets, Mo and TiN have been used to inhibit the coarsening of grains.<sup>19</sup>

Recently, a new alloy field “high-entropy alloys (HEAs)” has been developed in which each HEA contains at least five major elements with the concentration of each element being between 35 at.% and 5 at.%.<sup>20–25</sup> They have four core effects: high entropy, severe lattice distortion, sluggish diffusion, and cocktail effects and have a wide spectrum of properties. Suitable alloy design could give promising properties for different applications, such as high hardness, softening resistance to high temperature, wear resistance, and corrosion resistance. Based on these findings, some of them could be good candidates as binders for cemented carbides and cermets to improve properties and reduce cost. From these candidates, Al<sub>0.5</sub>CoCrCuFeNi HEA with a face-centered cubic (FCC) structure has been newly reported to be a promising binder for wetting WC and inhibiting WC coarsening. The sintered WC/HEA thus displays a higher hardness–toughness level at room temperature and a higher hot hardness than sintered WC/Co.<sup>26</sup> Similarly, this study is interested in FCC Co<sub>1.5</sub>CrFeNi<sub>1.5</sub>Ti<sub>0.5</sub> HEA, which has higher contents of Ni, Cr, and Ti for wetting TiC during LPS and high hardness and toughness to be a strong binder.<sup>27,28</sup> Therefore, with an aim of developing new TiC/Co<sub>1.5</sub>CrFeNi<sub>1.5</sub>Ti<sub>0.5</sub> cermets with superior properties, this study investigated its sintered microstructure, hardness and toughness, and that of typical TiC/Ni and TiC/Ni<sub>13</sub>Mo<sub>7</sub> cermets for comparison. In addition, morphology and coarsening behavior of TiC grains during LPS in these three binders are compared in terms of coarsening rate and coarsening mechanism.

## EXPERIMENTAL PROCEDURE

First, Co<sub>1.5</sub>CrFeNi<sub>1.5</sub>Ti<sub>0.5</sub> HEA powder (designated as T12 powder) was synthesized from elemental powders by ball milling. The can and balls used for ball milling were made of SKD11 tool steel and SUJ2 bearing steel, respectively. The elemental powders, which had purities >99%, were weighed and then put into the can with the milling balls in a glove box with protective argon atmosphere. Milling was conducted for 12 h with a high-energy ball milling machine, SPEX 8000D Mixer/Miller. Then, high-purity (>99%) TiC particles with an average particle size of 2 μm and the T12 HEA powder were mixed and milled under the same conditions as above for another 12 h. This time was chosen on the basis that it would provide effective pulverization of the TiC particles and uniform mixing between the two powders. Five composite powders were prepared with the compositions: TiC + 10 wt.%T12, TiC + 15 wt.%T12, TiC + 20 wt.%T12, TiC + 30 wt.%T12, and TiC + 40 wt.%T12. Finally, 2 wt.% of liquid paraffin and petroleum ether were added to the mixed powders and they were horizontally wet-milled for a further 24 h. For comparative purposes, two conventional compositions of TiC + 20%Ni and TiC + 20%Ni<sub>13</sub>Mo<sub>7</sub> were prepared using the same process and conditions. The milled powders were pressed into disk-like compacts (12.7 mm in diameter by 2.5 mm in thickness) using a biaxial pressure of 65 MPa. The compacts were de-waxed by heating them in an Ar + 10% H<sub>2</sub> atmosphere under a pressure of 100 Pa at 300°C and 500°C for 0.5 and 1 h, respectively. Subsequently, degassing was performed under vacuum at 1250°C for 1 h and vacuum sintering was then carried out at 1380°C, 1400°C, 1420°C, and 1450°C for 1 h, respectively. After sintering, the specimens were furnace-cooled to room temperature. Calibration of the sintering temperature was made to ensure that all sintering was carried out above the liquidus temperature of the T12 powder, which was 1351°C determined by a Perkin Elmer Diamond thermogravimetric/differential thermal analysis (TG/DTA) system.

Sintered specimens were ground sequentially by #400, #1000, and #2000 diamond disks and then polished with 1-μm diamond suspension. Composite powders without sintering were also embedded in the thermosetting resin under vacuum and prepared with the same procedure for metallographic observation. Microstructure was investigated with a JEOL-5410 scanning electron microscope (SEM). The average TiC grain size was obtained from the SEM images with the conventional line interception technique. For each specific condition, data were obtained from three images. Vickers hardness measurements of sintered specimens after metallographic grinding and polishing were made using a hardness testing machine (Mitutoyo HM-115) with a load of 30 kg and a duration time of 15 s. Seven points were taken for indentation to obtain an

average. The fracture toughness  $K_{IC}$  was calculated with the following equation.<sup>29</sup>

$$K_{IC} \left( \text{MPa m}^{-1/2} \right) = 0.15(\text{HV}/L)^{0.5}$$

where  $L$  (mm) is the summation of the crack lengths at the four corners of indentation.

## RESULTS AND DISCUSSION

### Microstructure and Mechanical Properties

Table I shows the hardness and fracture toughness of sintered TiC + 20%T12, TiC + 20%Ni, and TiC + 20% (Ni<sub>13</sub>Mo<sub>7</sub>).

Other data from analyzing a commercial TiC-cermet insert and from literature<sup>30</sup> on TiC cermets are also listed for comparison. It can be seen that the present TiC + 20%T12 cermet with HEA binder has the best properties because it is much harder than experimented and reported TiC + 20%Ni cermets although less tough in  $K_{IC}$ . In addition, it has higher hardness by at least HV 200 than experimented TiC + 20% (Ni<sub>13</sub>Mo<sub>7</sub>) and commercial TiC-cermet while at a similar toughness level. The main reason for this best property combination is the fine and dense structure of TiC + 20%T12 cermet. Figure 1 compares the microstructure of the experimented TiC + 20%T12, TiC + 20%Ni, and TiC + 20% (Ni<sub>13</sub>Mo<sub>7</sub>) cermets. All sintered specimens are seen to be highly densified by the LPS process. The

gray and white regions of the SEM micrographs are the TiC grains and matrix materials, respectively. For each binder, the TiC grains are seen to be dispersed uniformly in the matrices without the obvious presence of pores. This demonstrates the good wettability between TiC grains and all three binders. By the linear interception method, the grain sizes of sintered composites are calculated to be 0.87  $\mu\text{m}$ , 2.16  $\mu\text{m}$ , and 1.77  $\mu\text{m}$ , respectively. It is noted that the HEA binder not only provides the finest TiC grains but also renders the grains mostly round in shape. These two features are beneficial for hardness and toughness, and thus, they yield the best property combination among the three binders.

### Wettability

As for the wettability of Ni<sub>13</sub>Mo<sub>7</sub> and HEA binders, there are some differences from observation. It has been known that the wettability of Ni<sub>13</sub>Mo<sub>7</sub> comes from the formation of (Ti, Mo)<sub>x</sub>C<sub>1-x</sub> solid solution at the outer surface and thus the core-rim structure of TiC grains.<sup>16-18</sup> Such a core-rim structure is also clearly observed by comparing Fig. 1a and c. On the other hand, the evidence of the core-rim structure is not seen in the HEA binder case. The wettability of the HEA binder on TiC could be understood from the chemical analysis on some large TiC grains as shown in Fig. 2. The chemical composition at point A near the boundary was analyzed by EDS to be Ti: 97.73, Co: 0.23, Cr: 1.72, Fe: 0.02, and Ni: 0.30 in weight percentage based on metal elements; i.e., carbon content is neglected. The distribution of each metal element from one side to another side was analyzed by Line-scan, which indicates that the carbide former Cr from the binder matrix has a small and roughly constant concentration throughout the grain except the center region, whereas non-carbide formers, Co, Fe, and Ni, penetrate a small distance and reach to nearly zero level after crossing a boundary layer, whose thickness is about 0.5  $\mu\text{m}$  for this large grain. This small concentration of Cr incorporated during grain growth agrees with the small solubility of solute Cr-carbide in solvent TiC mainly because of their large difference in crystal structure.<sup>31</sup> On the other hand, Co, Ni, and Fe could not dissolve in the TiC grain because of their positive mixing enthalpy when

**Table I. Hardness and fracture toughness of sintered TiC + 20%T12, TiC + 20%Ni, and TiC + 20%(Ni<sub>13</sub>Mo<sub>7</sub>) (other data are also listed for comparison)**

Cermets	HV <sub>30</sub>	$K_{IC}$ (MPa m <sup>-1/2</sup> )
TiC + 20%T12	1876	9.0
TiC + 20%Ni	1372	11.8
TiC + 20%Ni [30]	1295	11.1
TiC + 20%(Ni <sub>13</sub> Mo <sub>7</sub> )	1639	8.5
CommercialTiC Cermet <sup>a</sup>	1685	9.1

<sup>a</sup>The composition in weight percentage is (TiC,WC,TaC) + 20% (Ni,Co,Mo), in which TiC:WC:TaC = 16:2:2 and Co:Ni:Mo = 5:3:2.

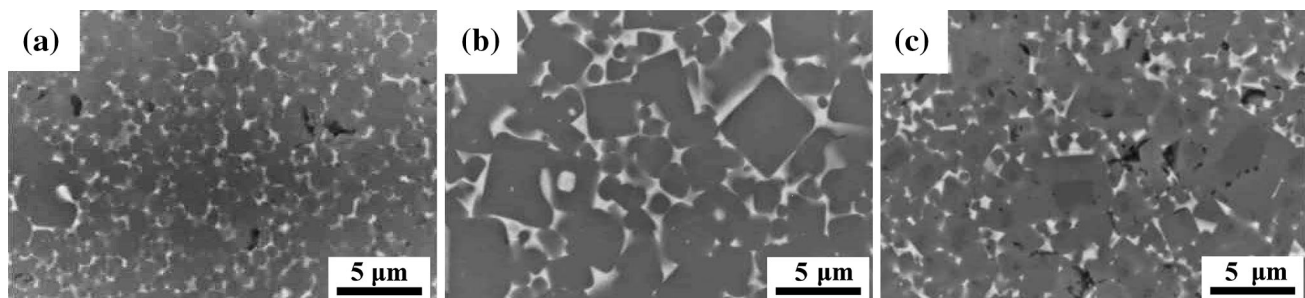


Fig. 1. SEM micrographs of (a) TiC + 20%T12, (b) TiC + 20%Ni, and (c) TiC + 20%Ni<sub>13</sub>Mo<sub>7</sub> cermets sintered at 1380°C.

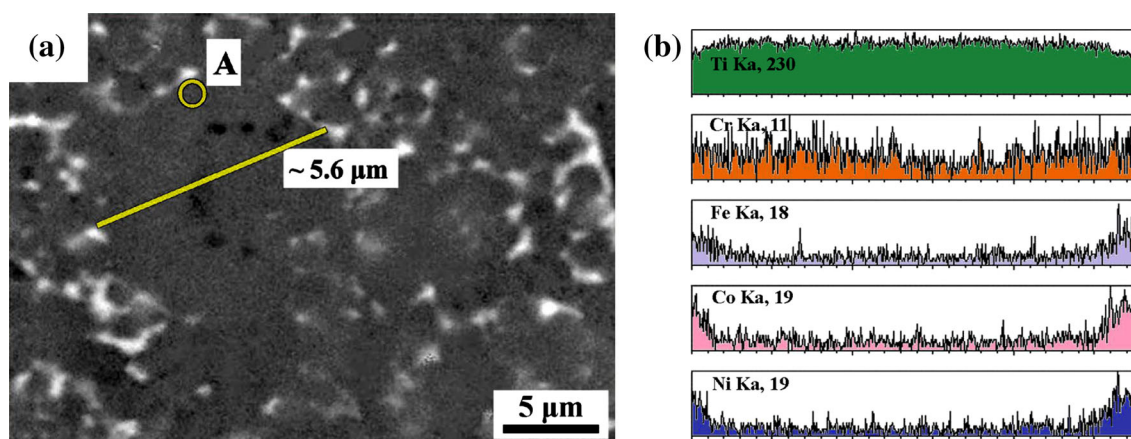


Fig. 2. (a) SEM analysis of point marked by A and (b) EDS analysis of line scan analyses for each metal element along the line about 5.6  $\mu\text{m}$  in length across a large grain found in TiC + 20%T12 cermet after sintering at 1380°C.

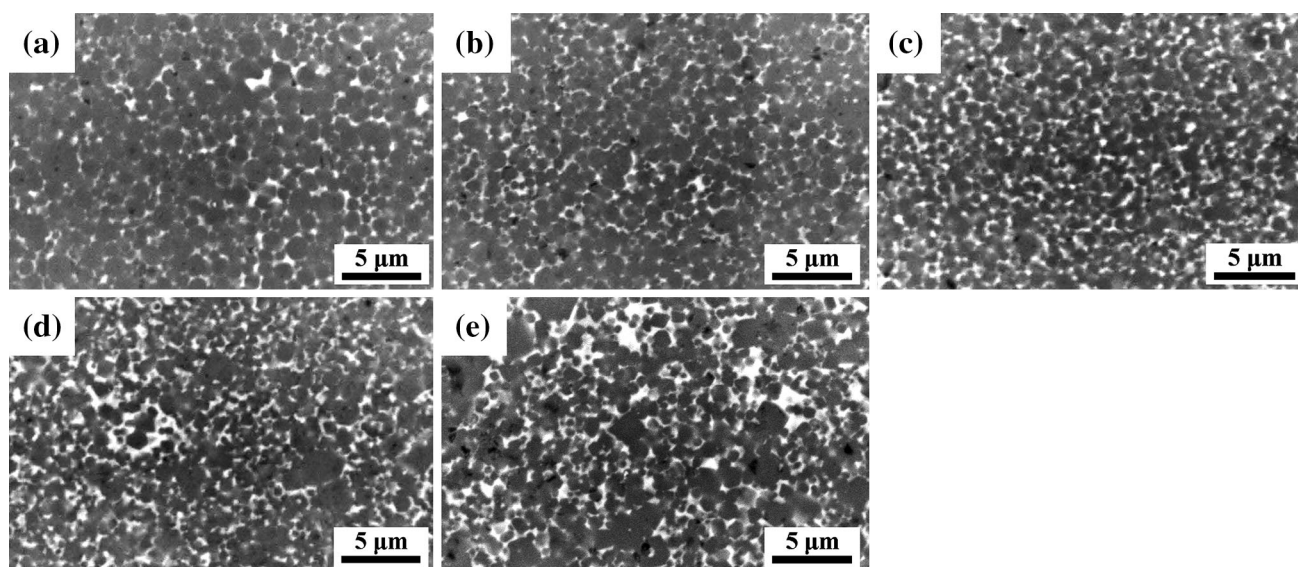


Fig. 3. SEM micrographs of TiC + (10–40)%T12 cermets sintered at 1380°C: (a) 10%, (b) 15%, (c) 20%, (d) 30%, and (e) 40%.

binding with carbon. Thus, it can be understood that there is a layer formed with the similar composition at point A during growth, and only about 2 at.% Cr (based on metal elements) could be incorporated into the new formed TiC layer (Co, Fe, and Ni are negligible in amount). Apparently, the multi-element containing boundary layer accounts for the wettability between HEA and TiC grains.

### Coarsening Kinetics and Coarsening Rate Analysis

The remarkably slow coarsening rate in the HEA binder was further analyzed to determine its growth kinetics. Figure 3 shows the microstructure of TiC/HEA cermets with different HEA volume fractions. Spherical grains are generally seen except some large faceted grains. Through closer inspection, it can be ascertained that larger grains tend to have a

faceted shape and the number of faceted grains increases with greater content of the HEA binder. This is reasonable because larger grains have received more growth volume to adjust their shape to attain their equilibrium faceted shapes during LPS. The existence of a large fraction of spherical grains also suggests that the interface energy of atomic planes would be significantly lowered in the HEA liquid so that the deviation between typical facet planes and those non-facet planes becomes small and has no large tendency to take the facet shape. On the other hand, the deviation is large in both Ni and Ni<sub>13</sub>Mo<sub>7</sub> liquids because their small grains already have clear facets. The fact that HEA liquid could significantly lower the surface energy of TiC grain could be attributable to the formation of the boundary layer mentioned above. This boundary layer provides a transition region between HEA liquid and TiC grains instead of an abrupt change in composition.

The average TiC grain sizes of these TiC/HEA cermets before and after sintering are listed in Table II.

It can be seen that the average size (in radius) of TiC grains in the composite powder before sintering increases with the amount of T12 powder. This tendency is due to the presence of the alloy binder that reduces the comminuting efficiency of the brittle TiC grains during ball milling. However, the average grain sizes of the five HEA contents after sintering are quite close to each other, from 0.435  $\mu\text{m}$  to 0.50  $\mu\text{m}$ . This demonstrates that the particle coarsening rate is slower for a higher volume fraction of HEA liquid. From the kinetics criterion of the effect of volume fraction on the coarsening rate mentioned in the Introduction section, the HEA binder obviously obeys diffusion-controlled kinetics during LPS.<sup>14,15</sup> As for the kinetics involved in the cermets with Ni and Ni<sub>13</sub>Mo<sub>7</sub> binders, Moon et al.<sup>15</sup> studied the mixed shape of carbide grains and concluded that the kinetics in Ni and Ni<sub>13</sub>Mo<sub>7</sub> liquid binders were diffusion-controlled because their large grains not only

have facets but also round corners and, moreover, that small grains have a larger portion of a round surface. Although the reason for mixed shape having diffusion-controlled kinetics was not explained further in Ref. 15, the present study proposes a reasonable mechanism for explaining this. When a large grain has facets in company with round corners and edges, the faster outward movement of atomically rough corners and edges by an advance relative to facets will create jogs that are easy to move laterally over the facets and thus cause the facets to advance a similar step. Hence, the overall growth of large grains is diffusion-controlled by the movement of the round surface. On the other hand, the inward movement of round edges of small grains also creates jogs that are easier to move laterally across the facets and result in the shrinkage and dissolution. Hence, the dissolution is again diffusion-controlled by the movement of a round surface. Therefore, growth of large grains and dissolution of small grains are all diffusion-controlled.

As the coarsening kinetics are all diffusion-controlled, the following coarsening equations from the LSW theory can be used.<sup>11,12,15,32</sup>

$$r^3 - r_0^3 = k_R t \quad (1)$$

$$v = \frac{dr}{dt} = \frac{k_R}{3r^2} \quad (2)$$

where  $r_0$  and  $r$  are the average grain radius before and after sintering,  $k_R$  is the coarsening rate constant,  $t$  is the growing time, and  $v$  is the coarsening rate.

Table III lists the average grain sizes (in radius) of TiC before and after sintering for TiC + 20%T12, TiC + 20%Ni, and TiC + 20%Ni<sub>13</sub>Mo<sub>7</sub> composites.

**Table II. Average grain sizes (in radius) of TiC before and after sintering at 1380°C for TiC + (10–40)%T12 cermets**

Amount of T12 binder (%)	Average size of TiC grains ( $\mu\text{m}$ )	
	Before sintering	After sintering
10	0.205	0.455
15	0.25	0.435
20	0.26	0.435
30	0.325	0.455
40	0.39	0.50

**Table III. Average grain sizes (in radius) of TiC before and after sintering at different temperatures for TiC + 20%T12, TiC + 20%Ni, and TiC + 20%Ni<sub>13</sub>Mo<sub>7</sub> cermets**

Sintering temperature (°C)	TiC + 20%T12		TiC + 20%Ni		TiC + 20%Ni <sub>13</sub> Mo <sub>7</sub>	
	$r_0$ ( $\mu\text{m}$ )	$r$ ( $\mu\text{m}$ )	$r_0$ ( $\mu\text{m}$ )	$r$ ( $\mu\text{m}$ )	$r_0$ ( $\mu\text{m}$ )	$r$ ( $\mu\text{m}$ )
1380	0.26	0.435	0.33	1.08	0.28	0.885
1400	0.26	0.53	0.33	1.14	0.28	0.925
1420	0.26	0.685	0.33	1.295	0.28	1.16
1450	0.26	0.875	0.33	1.39	0.28	1.34

**Table IV. TiC + 20%T12, TiC + 20%Ni, and TiC + 20%Ni<sub>13</sub>Mo<sub>7</sub> cermets**

	Coarsening rate constants $k_R$ ( $10^{-5} \mu\text{m}^2/\text{s}$ )				Activation energy (kJ/mol)
	1380°C	1400°C	1420°C	1450°C	
TiC + 20%T12	1.8	3.65	8.4	18.1	788.8
TiC + 20%Ni	34.0	40.2	59.3	73.6	265.3
TiC + 20%Ni <sub>13</sub> Mo <sub>7</sub>	18.7	21.4	42.8	66.2	422.4

The sintering temperatures are 1380°C, 1400°C, 1400°C, and 1450°C. The coarsening rate constants calculated from Eq. [2] for TiC grains in the different binders are given in Table IV.

A much smaller coarsening rate constant for the HEA binder than for the conventional binders can be seen regardless of the sintering temperature. This again confirms that the coarsening during LPS is significantly inhibited by the use of the Co<sub>1.5</sub>CrFeNi<sub>1.5</sub>Ti<sub>0.5</sub> HEA binder.

### Explanation for Coarsening Rate Difference

As the coarsening rate constant is proportional to the surface energy ( $\gamma$ ), equilibrium solubility ( $X_e$ ) of very large grains, and diffusion coefficient ( $D$ ),<sup>31</sup> the lowest coarsening rate in the HEA binder could be explained from these three factors.

The first factor has been mentioned in the discussion of wettability, in which the existence of a large fraction of spherical grains has suggested that the interface energy of atomic planes would be significantly lowered in the HEA liquid as compared with Ni and Ni<sub>13</sub>Mo<sub>7</sub> liquids because small grains of the latter two have a much higher fraction of facet area. In addition, the lowest interface energy is attributable to the formation of a boundary layer providing a transition region between HEA liquid and TiC grains instead of an abrupt change in composition. For the second factor of equilibrium solubility of very large grains, as the HEA binder already contains 9.1 at.%Ti, it is expected that TiC is more difficult to dissolve in the binder during coarsening. Thus, the equilibrium solubility factor also benefits the low coarsening rate of TiC grains in the HEA liquid binder. The third factor of the diffusion coefficient could be further analyzed with the activation energy of diffusion. As the coarsening rate constant ( $k_R$ ) is proportional to diffusion constant ( $D$ ), it satisfies the Arrhenius relationship and can be expressed by the following:<sup>10,15,32</sup>

$$k_R = k_{R_0} \exp\left(\frac{-Q}{RT}\right) \quad (3)$$

in which  $k_{R_0}$  is a temperature-independent constant and  $Q$  is the activation energy for coarsening. From Table IV, the plots of  $\log k_R$  against  $1/T$  for TiC + 20%Ti<sub>12</sub>, TiC + 20%Ni, and TiC + 20%Ni<sub>13</sub>Mo<sub>7</sub> cermets sintered at temperatures between 1380°C and 1450°C are shown in Fig. 4. It can be seen that each cermet has a good linear fit to the data points. The activation energies determined from the gradients of the plots in Fig. 4 are also given in Table IV. The activation energy of TiC + 20%Ti<sub>12</sub> is found to be considerably higher than that of either TiC + 20%Ni or TiC + 20%Ni<sub>13</sub>Mo<sub>7</sub>. Such a high value of activation energy appears to be very high in known LPS systems; for example, the typical activation energy of carbide system ranges from 84 kJ/mol to 167 kJ/mol in the diffusion-controlled process of WC in Co,<sup>15</sup> whereas those

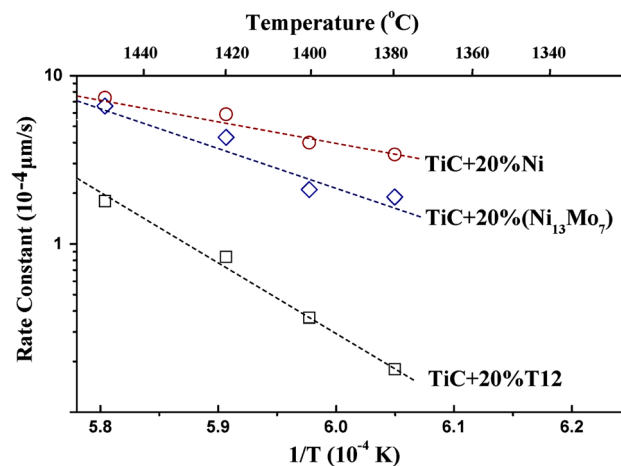


Fig. 4.  $\log k_R$  versus  $1/T$  plots for TiC + 20%Ti<sub>12</sub>, TiC + 20%Ni, and TiC + 20%Ni<sub>13</sub>Mo<sub>7</sub> cermets.

in the interface-controlled process range from 356 kJ/mol to 741 kJ/mol.<sup>33</sup> Although the activation energy data of TiC cermets is difficult to find in the literature, the activation energy, 265.3 kJ/mol, of TiC + 20%Ni can be understandable because TiC has stronger binding than WC and the Ti-Ni pair also has stronger bonding than W-Co. These stronger bondings would cause a slower dissolution rate of TiC and a slower diffusion rate of Ti in Ni liquid than that of WC and that of W in Co, respectively. As Mo is incorporated into the Ni binder, its low mobility because of its high melting point and its stronger binding with C would further cause the diffusion rate of Ti and C to be lower and the activation energy to be higher as observed in TiC + 20%Ni<sub>13</sub>Mo<sub>7</sub>. In the Co<sub>1.5</sub>CrFeNi<sub>1.5</sub>Ti<sub>0.5</sub> HEA binder, the higher content of carbon-strong-binding elements, Ti and Cr, would have an even larger effect on reducing the diffusion rate of Ti and C.

Two more factors, cooperative diffusion and higher packing density, also cause a lower diffusion rate. Although sluggish diffusion has been regarded to be a core effect in the whole-solute matrix of HEAs and verified by the diffusion couple experiments in the FCC Co-Cr-Fe-Mn-Ni alloy system,<sup>34</sup> the diffusion behavior in liquid state needs a different discussion. As the coarsening of TiC grains involves the mass transfer of TiC, the activation energy,  $Q$ , obtained from the coarsening data is equivalent to the activation energy of Ti and C species in the binder liquid. Diffusion in the HEA binder liquid is expected to be slow as a result of two factors: (i) the requirement of more difficult cooperative diffusion in the multi-elemental mixture because the diffusion of Ti from small grains to large grains needs other binder elements to cause diffusion in an opposite direction, and (ii) the reduced diffusion rate due to the higher packing density and thus viscosity of a liquid with different-size atoms because the diffusion in liquid is empirically proportional to viscosity.<sup>35</sup> Such arguments regarding

diffusion kinetics have been used to explain the high glass-forming ability of bulk metallic glasses and to justify Inoue's first rule requiring at least three elements.<sup>35</sup> From topological and chemical points of view, there is an increase in the degree of dense random packed structure and viscosity, which make atomic rearrangement and diffusion of atoms difficult. Therefore, a low diffusion coefficient due to the above factors benefits the low coarsening rate of TiC grains in the HEA binder. However, the present discussion is still qualitative. Further research to get more data and evidence is still required to have a clear understanding.

## CONCLUSION

New TiC/Co<sub>1.5</sub>CrFeNi<sub>1.5</sub>Ti<sub>0.5</sub> cermet has been developed with the HEA binder, which has higher contents of Ni, Cr, and Ti for wetting TiC during LPS and provides high hardness and toughness to improve overall performance. Excellent wettability, a much finer grain structure, and improved hardness–toughness combination were obtained as compared with two traditional binders, Ni and Ni<sub>13</sub>Mo<sub>7</sub>. Therefore, Co<sub>1.5</sub>CrFeNi<sub>1.5</sub>Ti<sub>0.5</sub> is an excellent HEA binder for TiC cermets. The low surface energy of TiC grains in the HEA binder, which enhances the wettability between liquid phase and TiC grains, is found to be due to the formation of a multi-element containing boundary layer. From the coarsening behavior of TiC grains, the coarsening kinetics of TiC grains in the three binders is diffusion-controlled. The activation energies of TiC + 20%Co<sub>1.5</sub>CrFeNi<sub>1.5</sub>Ti<sub>0.5</sub>, TiC + 20%Ni, and TiC + 20%Ni<sub>13</sub>Mo<sub>7</sub> are 788.8 kJ/mol, 265.3 kJ/mol, and 456.1 kJ/mol, respectively. The high activation energy of the Co<sub>1.5</sub>CrFeNi<sub>1.5</sub>Ti<sub>0.5</sub> binder was attributable to higher content of carbon-strong-binding elements, Ti and Cr, which reduced the diffusion rate of Ti and C. In addition, the sluggish diffusion of HEA liquid due to cooperative diffusion and higher packing density of multiple different-sized atoms is also a factor to increase activation energy and thus reduce the diffusion rate. A low diffusion coefficient, low surface energy, and low solubility of Ti in the HEA binder explains the slow coarsening of TiC grains.

## ACKNOWLEDGEMENTS

The authors are pleased to acknowledge the financial support for this research by the Ministry of Science and Technology of Taiwan under Grant No. MOST 103-2218-E-007-011.

## REFERENCES

1. B. Wittmann, W.D. Schubert, and B. Lux, *Int. J. Refract. Met. Hard Mater.* 20, 51 (2002).
2. D.F. Carroll, *Int. J. Refract. Met. Hard Mater.* 17, 123 (1999).
3. I.M. Stephenson and J. White, *Trans. Br. Ceram. Soc.* 66, 443 (1967).
4. K.W. Kay, *J. Am. Ceram. Soc.* 51, 373 (1967).
5. N.C. Kothari, *J. Less-Common Met.* 13, 457 (1967).
6. H. Fischmeister, A. Kannappan, L.H. Yi, and E. Navara, *Phys. Sinter.* 1, 1 (1969).
7. R. Warren, *J. Mater. Sci.* 3, 471 (1968).
8. W. May, *J. Mater. Sci.* 6, 1209 (1971).
9. H.E. Exner, E.S. Marta, and G. Petzow, *Modern Developments in Powder Metallurgy: Process*, Vol. 4 (New York, NY: Plenum Press, 1971), p. 315.
10. R. Warren, *J. Mater. Sci.* 7, 1434 (1972).
11. I.M. Lifshitz and V.V. Slyozov, *J. Phys. Chem. Solids* 19, 35 (1961).
12. Z.C. Wagner, *Electrochemistry* 65, 581 (1961).
13. M. Hillert, *Phase Equilibria, Phase Diagrams and Phase Transformations: Their Thermodynamic Basis* (New York, NY: Cambridge University Press, 1998), p. 149.
14. H. Ye, V. Pujar, and N.P. Padture, *Acta Mater.* 47, 481 (1999).
15. H. Moon, B. Kim, and S.L. Kang, *Acta Mater.* 48, 1293 (2001).
16. K. Oh, J. Jun, and D. Kim, *J. Am. Ceram. Soc.* 83, 3117 (2000).
17. D.A. Porter and K.E. Easterling, *Phase Transformation in Metals and Alloys*, 2nd ed. (London: Chapman & Hall, 1992), pp. 168–180.
18. W.D. Schubert, A. Bock, and B. Lux, *Int. J. Refract. Met. Hard Mater.* 13, 281 (1995).
19. V.A. Tracey, *Int. J. Refract. Met. Hard Mater.* 11, 137 (1992).
20. J.W. Yeh, S.K. Chen, S.J. Lin, J.Y. Gan, T.S. Tsau, and S.Y. Chang, *Adv. Eng. Mater.* 6, 299 (2004).
21. J.W. Yeh, *J. Met.* 65, 1759 (2013).
22. Y. Zhang, T.T. Zuo, Z. Tang, M.C. Gao, K.A. Dahmen, P.K. Liaw, and Z.P. Lu, *Prog. Mater. Sci.* 61, 1 (2014).
23. M.H. Tsai and J.W. Yeh, *Mater. Res. Lett.* 1, 207 (2014).
24. M.C. Gao and D.E. Alman, *Entropy* 15, 4504 (2013).
25. Y. Zhang, et al., *Prog. Mater. Sci.* 61, 1 (2014).
26. C.S. Chen, C.C. Yang, H.Y. Chai, J.W. Yeh, and J.L.H. Chau, *Int. J. Refract. Met. Hard Mater.* 43, 200 (2014).
27. Y.L. Chou, J.W. Yeh, and H.C. Shih, *Corrosion* 67, 085002 (2011).
28. M.H. Chuang, M.H. Tsai, W.R. Wang, S.J. Lin, and J.W. Yeh, *Acta Mater.* 59, 6308 (2011).
29. W.D. Schubert, H. Neumeister, G. Kinger, and B. Lux, *Int. J. Refract. Met. Hard Mater.* 16, 133 (1998).
30. R. Koc, C. Meng, and G.A. Swift, *J. Mater. Sci.* 35, 3131 (2000).
31. H.O. Pierson, *Handbook of Refractory Carbides and Nitrides* (Upper Saddle River, NJ: Noyes Publications, 1996), p. 69.
32. D.A. Porter and K.E. Easterling, *Phase Transformation in Metals and Alloys*, 2nd ed. (London: Chapman & Hall, 1992), pp. 314–317.
33. I. Konyashin, S. Hlawatschek, B. Ries, F. Lachmann, F. Dorn, A. Sologubenko, and T. Weirich, *Int. J. Refract. Met. Hard Mater.* 27, 234 (2009).
34. K.Y. Tsai, M.H. Tsai, and J.W. Yeh, *Acta Mater.* 61, 4887 (2013).
35. A. Inoue, *Acta Mater.* 48, 279 (2000).